Experimental Research

INTERNATIONAL JOURNAL OF SURGERY

OPEN

Tracking adipose-derived stem cell exosomes applied in a mouse crush injury model: insights from fluorescent labeling and spatial transcriptomics – an experimental study

Cheng-Shyuan Rau, MD[a], Shao-Chun Wu, MD[b], Pao-Jen Kuo, MD[c], Chia-Wei Lin, MSc[c], Tsu-Hsiang Lu, BA[c], Yi-Chan Wu, MSc[c], Chia-Wen Tsai, MSc[c], Ching-Hua Hsieh, MD, PhD[c,*]

Abstract

Adipose-derived stem cell exosomes (ADSC-exos) are promising for nerve regeneration; however, their precise mechanisms remain unclear. This study employed fluorescent labeling and spatial transcriptomics to track the effects of ADSC-exos on crushed sciatic nerves in mice. Labeled exosomes were detected in spinal neurons and proximal nerve segments after application. Spatial transcriptomics revealed significant changes in gene expression, with an upregulation of neurons and Schwann cells and the downregulation of oligodendrocytes. The key pathways affected were prosaposin, pleiotrophin, fibroblast growth factor, secreted phosphoprotein 1, SLIT and NTRK-like family, member, vascular endothelial growth factor, and growth arrest-specific protein. ADSC-exo treatment enhanced cell-cell interactions, particularly between Schwann cells and astrocytes, thereby promoting a regenerative environment. Gene ontology analysis suggested improvements in metabolic activity, cell communication, and structural support. This study highlights the complex interplay between multiple cell types and signaling pathways involved in the nerve regeneration response to ADSC-exos. This comprehensive approach offers new perspectives on the role of ADSC-exos in nerve regeneration and paves the way for advanced regenerative strategies for peripheral nerve injuries.

Keywords: adipose-derived stem cells (ADSCs), biorthogonal click chemistry, exosome, nerve crush injury, nerve regeneration, spatial transcriptome

Introduction

Peripheral nerve injuries are a substantial and challenging issue in both clinical practice and public health. These injuries often cause disability and loss of function[1,2]. Despite the availability of advanced microsurgical procedures, achieving a satisfactory level of functional recovery following the repair of peripheral nerves remains a formidable task[3-8]. Consequently, there is increasing interest in developing effective ways to promote nerve regeneration after such injuries. Numerous methodologies have been investigated in this field, including autologous or allogenous nerve grafts, synthetic conduits, stem cell applications, and exploitation of the therapeutic capabilities of extracellular vesicles released by cells. These interventions are currently the subject of extensive investigations[9,10].

Adipose-derived stem cells (ADSCs) play a pivotal role in nerve regeneration after injuries[11]. This effect may be attributed to several mechanisms such as the stimulation of robust Schwann cell proliferation[12], stem cell differentiation into Schwann-like cells[12], and the secretion of neurotrophic factors that enhance nerve regeneration[13]. Exosomes are key mediators of intercellular communication that affect a wide range of physiological and pathological processes[14]. It has been reported that adipose-derived stem cell exosomes (ADSC-exo) effectively enhance nerve regeneration by optimizing Schwann cell functionality[15]. ADSC-exos contain various neural growth factors that facilitate Schwann cell proliferation[16,17] and migration by downregulating the phosphatase and tensin homolog (PTEN)[18]. They also mitigate Schwann cell apoptosis[16,19], impede Schwann cell autophagy[20], and promote myelin sheath formation[20,21]. This provides new evidence that ADSC-exos may be useful for nerve regeneration therapeutics[17].

Our previous study using a mouse nerve crushed model revealed that local application of ADSC-exo to the injured nerve significantly enhanced the process of nerve regeneration[22].

[a]Department of Neurosurgery, Kaohsiung Chang Gung Memorial Hospital and Chang Gung University College of Medicine, Kaohsiung, Taiwan, [b]Department of Anesthesiology, Kaohsiung Chang Gung Memorial Hospital and Chang Gung University College of Medicine, Kaohsiung, Taiwan and [c]Department of Plastic Surgery, Kaohsiung Chang Gung Memorial Hospital and Chang Gung University College of Medicine, Kaohsiung, Taiwan

Cheng-Shyuan Rau and Shao-Chun Wu contributed equally to this work as the first authors.

Sponsorships or competing interests that may be relevant to content are disclosed at the end of this article.

*Corresponding author. Address: Department of Plastic Surgery, Kaohsiung Chang Gung Memorial Hospital and Chang Gung University College of Medicine, Kaohsiung 83301, Taiwan. Tel.: +886 7 3454746.
E-mail: Taiwanm93chinghua@gmail.com (C.-H. Hsieh).

International Journal of Surgery (2025) 111:1860–1873

Received 18 August 2024; Accepted 12 November 2024

Supplemental Digital Content is available for this article. Direct URL citations are provided in the HTML and PDF versions of this article on the journal's website, www.lww.com/international-journal-of-surgery.

Published online 20 December 2024

http://dx.doi.org/10.1097/JS9.0000000000002166

This was evident in the histomorphological analysis of nerve samples stained with toluidine blue on day 10 post-injury, in which we observed substantial improvements, including increased fiber and width, fiber, axon, myelin, and total fiber areas[22]. Furthermore, topical application of ADSC-exos significantly lowered macrophage autophagy in the spinal cord following sciatic nerve crush injury[23]. This study aimed to ascertain the potential effect of these exosomes on innervated neurons and cells in the spinal cord. To address these questions, we conducted experiments in a nerve-crush mouse model to trace the destinations of ADSC-exos labeled with fluorescent markers. Furthermore, we performed spatial transcriptome analysis of the innervated spinal cord segment to have a thorough understanding of the functional interplay between cells in the spinal cord after ADSC-exo treatment of the crushed sciatic nerve of the mouse. This study was conducted in accordance with the ARRIVE criteria[24].

Materials and methods

Culture of the mouse ADSCs

C57BL/6 mouse ADSCs, sourced from brown fat tissue, were supplied by iXCell Biotechnologies (San Diego, CA, USA). These cells were cultured in ADSC basal medium (catalog number MD-0003, iXCells Biotechnologies) according to the manufacturer's guidelines until a predefined cell count was reached for the experiments. Strict aseptic techniques were used for cell culture, and a Mycoplasma PCR Detection Kit (MP0035, Merck, Kenilworth, NJ, USA) was used to avoid contamination by mycoplasma. Flow cytometric analysis confirmed the presence of stem cell markers including CD73, CD90, and CD105, whereas the cells tested negative for CD3, CD11b, CD25, CD45, and CD106.

Fluorescence labeling by biorthogonal click chemistry

In vitro labeling and in vivo tracking of exosomes have been achieved using a one-step in situ fluorescent labeling method based on bioorthogonal click chemistry[25,26]. ADSCs were subjected to two different treatments: 0 M (0.1% DMSO, serving as a reference) and 50 M azido sugars, known as tetraacetylated N-azidoacetyl-d-mannosamine (Ac4ManNAz), obtained from Click Chemistry Tools (Scottsdale, AZ, USA). Through metabolic glycoengineering, artificial azide groups (–N3) were added to the cell surface. Following treatment, the cells were washed and grown for 1 day in phenol red-free DMEM before being labeled with 10 M cyanine dye 5 (Cy5) dye-conjugated dibenzylcyclooctyne (DBCO-Cy5, catalog number 777366; Sigma-Aldrich, St. Louis, MO, USA) using bioorthogonal click chemistry. This labeling process was performed for 1 h at a temperature of 37°C.

Fluorescent images were acquired using a confocal microscope (FLUOVIEW FV10i; Olympus, Tokyo, Japan) operating at excitation and emission wavelengths of 650 nm and 670 nm, respectively. Bright-field and fluorescent images were acquired at 200× magnification at different time intervals, namely, 0, 3, 6, 24, and 48 h after Cy5 labeling. Images were acquired in the presence of Vecta Shield Antifade Mounting Medium, which contained 4′,6-diamidino-2-phenylindole (DAPI) stain (Vector Laboratories, Newark, CA, USA).

Isolation of the exosomes secreted by mouse ADSCs

In this study, the third passage of ADSCs was used to isolate exosomes. Exosomes secreted by cultured mouse ADSCs were obtained after incubation with either 0 or 50 μM of Ac4ManNAz, followed by subsequent labeling with Cy5. Exosomes obtained from the ADSCs after 48 h were classified as control exosomes (control-exo) or Cy5-labeled exosomes (Cy5-exo).

The exosomes were extracted using the ExoQuick-TC™ exosome precipitation solution (System Biosciences, Mountain View, CA, USA) following the instructions provided by the manufacturer. This procedure included centrifuging the culture media, which held exosome concentrations ranging from 1×10^9 to 1×10^{10} exosomes in 100 μL of culture media, at 1500×g for 30 min. Subsequently, the supernatant was removed and an equivalent volume of phosphate-buffered saline (PBS) was used to resuspend the exosome pellet for further experiments. Following the guidelines outlined in the Minimal Information for Studies of Extracellular Vesicles 2022[27,28], the isolated exosomes were characterized as described in our previous study[22,23,29,30], which included the expression of positive exosomal surface markers, absence of the negative control protein calnexin, a cup-shaped appearance with lipid bilayers, acceptable quality in terms of morphology by transmission electron microscopy (TEM), and an acceptable size range in dynamic light scattering (DLS) measurements.

Animal nerve crush surgery model

Male C57BL/6 mice were purchased from the National Laboratory Animal Center of Taiwan. All housing conditions, surgical procedures, analgesia, and assessments were performed at a specific pathogen-free facility accredited by the Association for Assessment and Accreditation of Laboratory Animal Care International and followed both national and institutional requirements. The Institutional Animal Care and Use Committee (IACUC) of Chang Gung Memorial Hospital approved the animal protocols (approval numbers 2022031502 and 2023060702). The mice were not bred in-house and were kept in individually ventilated cages lined with autoclaved dust-free wood shavings, with 2-3 mice housed per cage. We maintain the mice under a 12-hour light/12-hour dark cycle, maintaining the housing temperature between 20°C and 24°C. Food and water were provided ad libitum. We established an animal model for nerve crush injury using male mice aged 8-12 weeks and weighing 20-30 g, based on our previous studies[22,23,31,32]. Mice were randomized and assigned to control or experimental groups, with six mice in each subgroup at each assessment time point. Experiments were performed on mice that received the same treatment simultaneously. Before the experiment, the mice underwent a health check to ensure that they were free of disease and suitable for the study. This included weighing, physical examination, and monitoring for signs of illness or distress. For the nerve crush model, anesthesia was administered using a mixture of 25 mg/kg ketamine and 50 mg/kg xylazine. The right sciatic nerve of each mouse was exposed at the mid-thigh level and No. 5 Jeweler forceps were used to provide consistent pressure on the nerves for 30 s. This nerve crush model is reliable for creating axonotmesis[33] and has been extensively used in the literature[22,23,31-36]. In this paradigm, the addition of ADSC-exos significantly increases nerve regeneration[15,22]. After the

experiment was concluded, the IACUC approved the humane euthanasia of mice using an anesthetic overdose. The study that revealed no adverse events were observed.

Immunohistochemical analysis following locally-sprayed exosomes

Immediately after crushing the nerve segment, a 30-gauge syringe needle (Becton-Dickinson & Co., Franklin Lakes, NJ, USA) was used to apply a solution that had 100 μg of Cy5-exo within 100 μL of PBS around the crushed area[22,23]. The control group consisted of mice with crushed nerves who had been treated with 100 μL of PBS. The L4-L6 spinal cords and nerve segments proximal to the crushed site in the mice were collected at time intervals of 1, 2, 4, and 24 h after treatment ($n = 6$ mice in each group). These specimens were subjected to immunohistochemical analysis to visualize fluorescence. The spinal and nerve segments were sliced into sections 8-μm thick. Frozen sections were rinsed with PBS-Tween20, followed by blocking with a solution containing PBS, 1% Triton X-100, and 5% bovine serum albumin. After staining with DAPI, the localization of fluorescent cells was observed using a FLUOVIEW FV10i confocal microscope (Olympus Corporation, Tokyo, Japan). The number of cells showing co-localization of DAPI and Cy5 was quantified across 20 randomly chosen fields in each sample at a magnification of 60×, and the results were presented as the average number of cells per field. One-way analysis of variance (ANOVA) was used to examine the overall differences between the means of the various groups. Post hoc Fisher's least significant difference test was used to conduct comprehensive comparisons. Data were presented as the average values with standard errors. The statistical significance level was set at $P < 0.05$.

Spatial transcriptome analysis

For spatial transcriptome analysis, the L4-L6 spinal cords of mice receiving 100 μg ADSC-exo in the experimental groups (ADSC-exo treatment group) or 100 μL of PBS (control group) were harvested 24 h later. Specimens were harvested 24 h after applying ADSC-exos or control PBS to the crushed nerve site in a mouse model of sciatic nerve crush injury. These tissues were sectioned to a thickness of 10 μm at –20°C using a Leica cryostat. These sections were mounted on highly adhesive slides and stained with hematoxylin and eosin (H&E) for sample selection and confirmation of the optimal position. Spatial gene expression in formalin-fixed, paraffin-embedded (FFPE) tissue sections in duplicate for the experimental and control groups ($n = 2$) was processed using 10x Genomics Visium CytAssist (10x Genomics Platform, Pleasanton, California, USA), following the manufacturer's protocol. Briefly, FFPE tissue sections were placed on positively charged slides. The sections were subjected to deparaffinization, H&E staining, imaging, and decrosslinking. Subsequently, whole transcriptome probe panels were applied to mice. Following probe hybridization, tissue slides, and Visium CytAssist Spatial Gene Expression V2 slides were loaded into the Visium CytAssist instrument. Spatially barcoded oligonucleotides released gene expression probes from the tissue and captured them on the Visium slide surface. The visium slide was then removed to prepare the downstream library. Probes were extended during library preparation by adding a unique molecular identifier (UMI), spatial barcode, and partial Read 1 primer. The polymerase chain reaction (PCR) amplification was conducted using the Applied Biosystems™ Veriti™ 96-Well Thermal Cycler, manufactured by Thermo Fisher Scientific in Waltham, MA, USA. The amplified products were purified using SPRIselect beads and converted into sequencing libraries, following the manufacturer's instructions. The libraries were sequenced using the Illumina NovaSeq platform. Sequencing involved read lengths of 150 bp for Read 1, which included a 16 bp single-cell barcode, a 10x barcode, and a 12 bp UMI. Read 2 was 150 bp long and contained a transcript insert. Additionally, the i7 index (sample index) had a length of 10 bp and the i5 index (sample index) had a length of 10 bp.

Raw FASTQ files were processed using the Space Ranger (v2.1.1) analysis pipeline to obtain a spatial gene expression matrix. Downstream analysis was conducted using R (v4.3.1). As each spot in Visium v2 may consist of more than one cell, spot deconvolution analysis was employed to infer the cell types or mixtures of cell types. We used three strategies to interpret the spots on the tissue slides. The results of the non-reference-based (Latent Dirichlet Allocation-based) spot deconvolution method[37] were then processed to perform gene ontology (GO) and Kyoto Encyclopedia of Genes and Genomes (KEGG) pathway enrichment analyses. These two enrichment analyses were conducted using ClusterProfiler (v4.8.3) to define the functions of each deconvolution topic. Robust cell-type decomposition (RCTD), another deconvolution method, has been used to reproduce known cell types and subtype localization patterns. This functionality was implemented using the SpaceXR (v2.2.1) package. The computational framework CellTrek (v0.0.94) was used to map individual cells back to their specific locations in the tissue slices. Mapping was performed using the scRNA-seq and spatial transcriptome data. A single-cell reference based on a well-annotated single-nucleus RNA dataset from the mouse lumbar spinal cord published in *Nature Communications*[38] was used for the RCTD and CellTrek analyses.

Cell-cell communication analysis

The Seurat tool was used to process the matrix of spatial transcriptome data. Following the usual approach, the CellChat (V1.6.1) program was used to identify and visualize cell-cell communication networks. Potential cell-cell interactions and cellular crosstalk were identified using CellChatDB, a complete database of ligand-receptor interactions and cell-cell communication networks. Network diagrams and heatmaps were used to demonstrate the significantly different cell-cell interactions between the groups.

Results

Exosome isolation and characterization

Western blot analysis of the Cy5-exo sample revealed a greater presence of positive exosomal surface markers, including CD9, CD81, TSG101, and Alix, compared to the control medium (Fig. 1A). In contrast, there was no detectable expression of the negative control protein calnexin (Fig. 1A). The TEM images revealed the presence of circular exosomes with lipid bilayers that met the size and morphological criteria (Fig. 1B). In addition, the size distribution of the isolated exosomes was remarkably consistent, highlighting the high quality of the isolates. The distribution of exosome size was evaluated by DLS, which

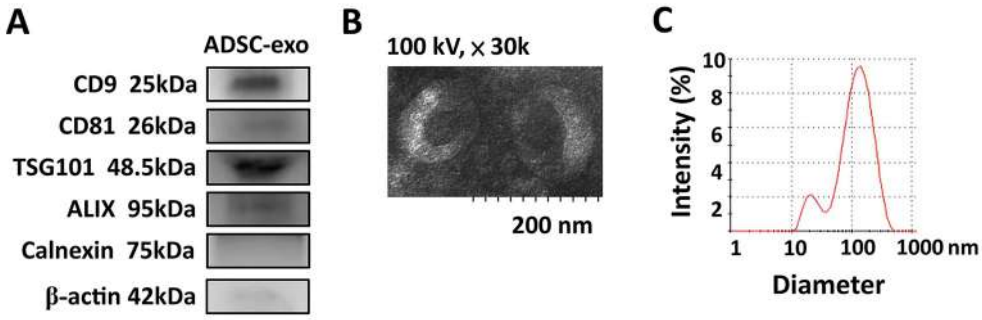

Figure 1. Exosome characterization. Isolated exosomes are assessed using (A) dynamic light scattering (DLS) to determine particle size and distribution in triplicate, (B) western blot analysis to identify exosomal surface markers in the isolated cyanine dye 5 (Cy5)-labeled exosomes using biorthogonal click chemistry (Cy5-exo), with the medium serving as the control, and (C) transmission electron microscopy (TEM).

showed an average size of 110.6 ± 48.6 nm. The distribution exhibited a single peak, and the polydispersity index was approximately 0.79 (Fig. 1C).

Fluorescence labeling by biorthogonal click chemistry

ADSCs typically exhibit a fibroblast-like morphology when observed under light microscopy as elongated spindle-shaped cells with small round nuclei, thin cytoplasmic extensions, and a relatively high nucleus-to-cytoplasm ratio (Fig. 2A). When the ADSCs were treated with Ac4ManNAz containing the azide group (–N3), the unnatural azide groups were incorporated into the surface of the ADSCs, making them glycoengineered ADSCs. The addition of the fluorescent reagent Cy5 enabled immediate in situ one-step labeling of the surfaces of these glycoengineered ADSCs. During endocytosis, the fluorescently labeled cell membrane invaginates, forming vesicles called early endosomes, which mature into late endosomes, also known as multivesicular bodies (MVBs). Certain MVBs merge with the cellular membrane and discharge exosomes that are labeled with fluorescent markers into areas outside the cell.

Following a 1-day incubation period, the presence of non-natural azide groups was visualized using 50-μM DBCO-Cy5 through the application of bioorthogonal click chemistry (Fig. 2B). Cy5 rapidly attached to glycoengineered ADSCs, with fluorescence readily apparent throughout the cells immediately after introduction of Cy5. This immediate labeling of Cy5 onto the azide group located on the cell surface was evident from subsequent images captured at 3, 6, 24, and 48 h, revealing the time-dependent emergence of Cy5-labeled exosomes (Cy5-exo). Most Cy5 fluorescence signals were observed on the surface of the ADSCs during the initial incubation period, ranging from 0 to 3 h. However, approximately 6 h after incubation, Cy5-labeled multivesicular bodies were formed in the cytoplasm. After 6 h, the red dots with Cy5-labeled signals were distributed throughout the cytoplasm, and after 24 h, they were distributed within the cytosol. At this time, the exosomes with a red color were observed to have been released from the cytoplasm and localized to the outer cell membrane. The aggregation of red-colored exosomes was observed with increased fluorescence intensity until the time point at 48 h. These observations suggest that 48 h following the addition of Cy5 to bioorthogonal click chemistry is a suitable time point for obtaining high yields of Cy5-labeled exosomes.

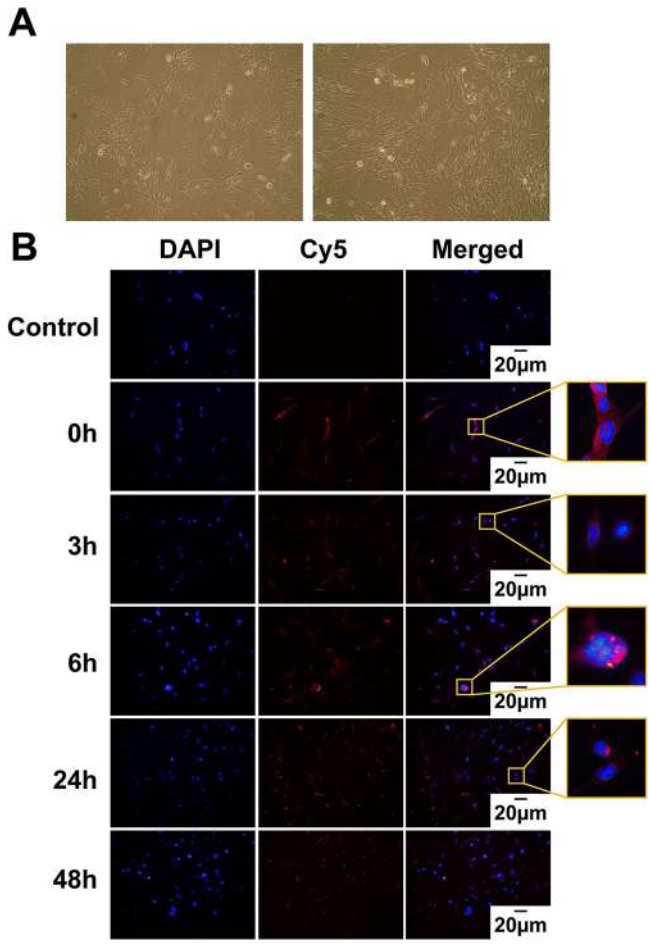

Figure 2. Fluorescence labeling using bioorthogonal click chemistry. (A) The typical fibroblast-like morphology of ADSCs under light microscopy with elongated spindle-shaped cells with small round nuclei and thin cytoplasmic extensions. (B) ADSCs are incubated with 50 μM of azido sugars, specifically tetraacetylated N-azidoacetyl-D-mannosamine (Ac4ManNAz), introducing the non-natural azide groups (-N3) onto their surface. Subsequently, they are labeled with 10 μM of cyanine dye 5 (Cy5). Fluorescence images are acquired at 0, 3, 6, 24, and 48 h, all at a magnification of 200×. DAPI (4′,6-diamidino-2-phenylindole) was used. The length of the scale bar measures 20 μm.

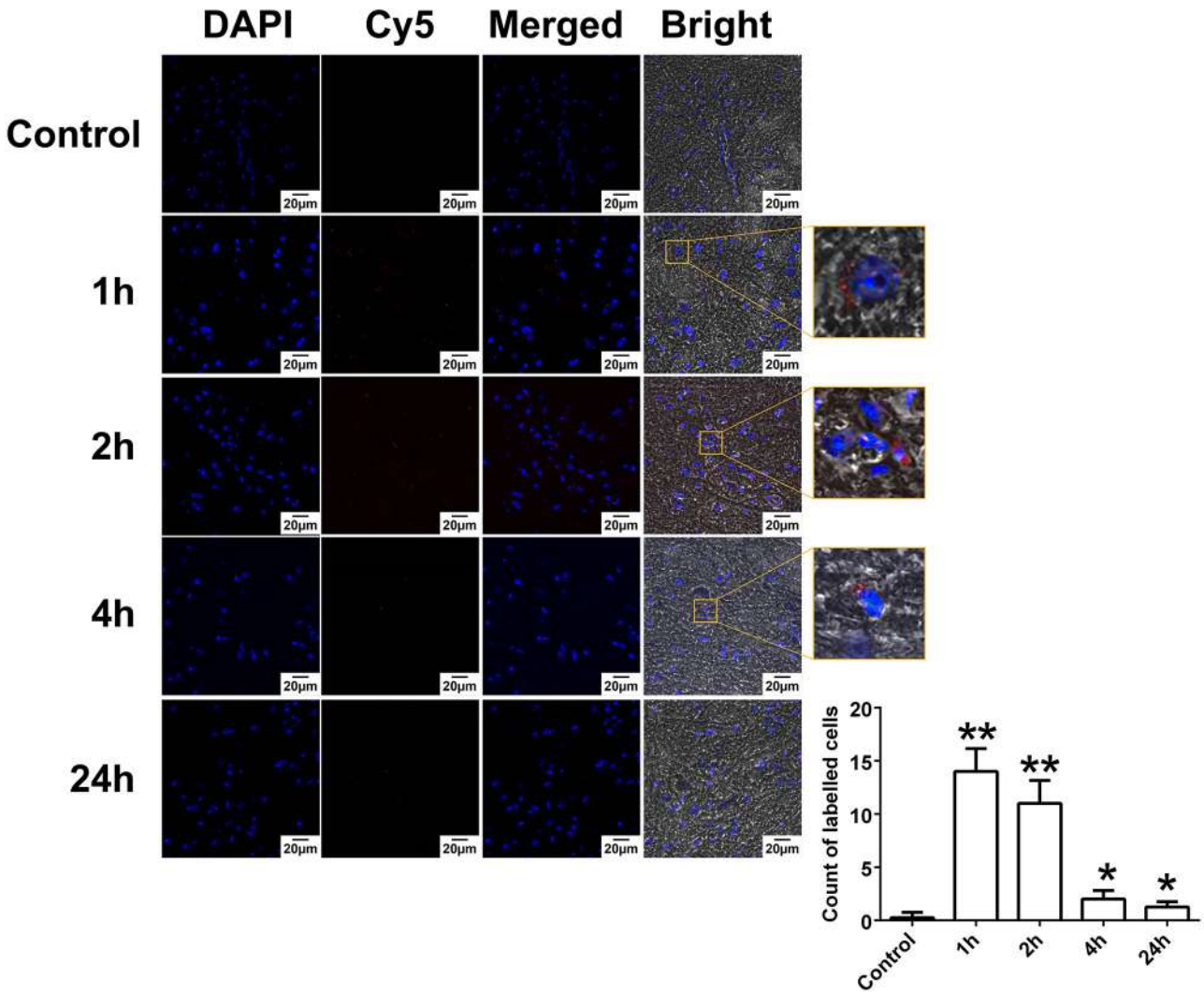

Figure 3. Immunohistochemical assessment of DAPI and Cy5 co-localization in the L4-L6 spinal cord of mice. Following the topical treatment with Cy5-exosomes in the nerve crush site, the quantification of DAPI+/Cy5+ cells is conducted across 20 randomly chosen fields within the L4-L6 spinal cord, all observed at a magnification of 60×. The results are shown as the average number of cells per field in a cross-section of the spinal cord. The symbols * and ** indicate significant changes ($P < 0.05$ and $P < 0.01$, respectively) compared to the control group. Error bars indicate the standard error of the mean. The length of the scale bar measures 10 μm.

Detection of Cy5-exo in the spinal cords

As shown in Fig. 3, quantification of the cells demonstrating the co-localization of DAPI and Cy5-exo within L4-L6 spinal cords revealed a significant rise in the average number of cells positive for both DAPI and Cy5 per field at 1 h (14.0 ± 1.1 cells/field) and 2 h (11.0 ± 1.1 cells/field) after the exosome application to the injured nerve, when compared with the control-exo group. This increase persisted for at least 24 h (1.25 ± 0.25 cells/field) following the ADSC-exo treatment. However, the number of cells exhibiting co-localization of DAPI and Cy5 markedly decreased at 4 h (2.00 ± 0.41 cells/field) after exosome treatment.

Detection of Cy5-exo in the proximal nerve segments

As shown in Fig. 4, the quantification of cells exhibiting co-localization of DAPI and Cy5-exo in the proximal nerve segments revealed that, in comparison to that of the control-exo group, the average number of cells positive for both DAPI and Cy5 per field has significantly increased at 1 h (3.2 ± 0.31 cells/field) and 2 h (1.9 ± 0.44 cells/field) following the application of ADSC-exo onto the injured nerve. However, at 4 h following exosome treatment, the number of DAPI+/Cy5+ cells (0.83 ± 0.21 cells/field) did not exhibit a significant difference compared to that of the control-exo group.

Spatial transcriptome analysis

We assessed the spatial distribution of different cell types by performing spatial transcriptome analysis on control and experimental (ADSC-exo) samples, which consisted of 641 and 810 spots, respectively. Spatial transcriptome sections of the samples were subjected to histological staining with H&E (Fig. 5A). Based on the spatial transcriptome sequencing data, distinct

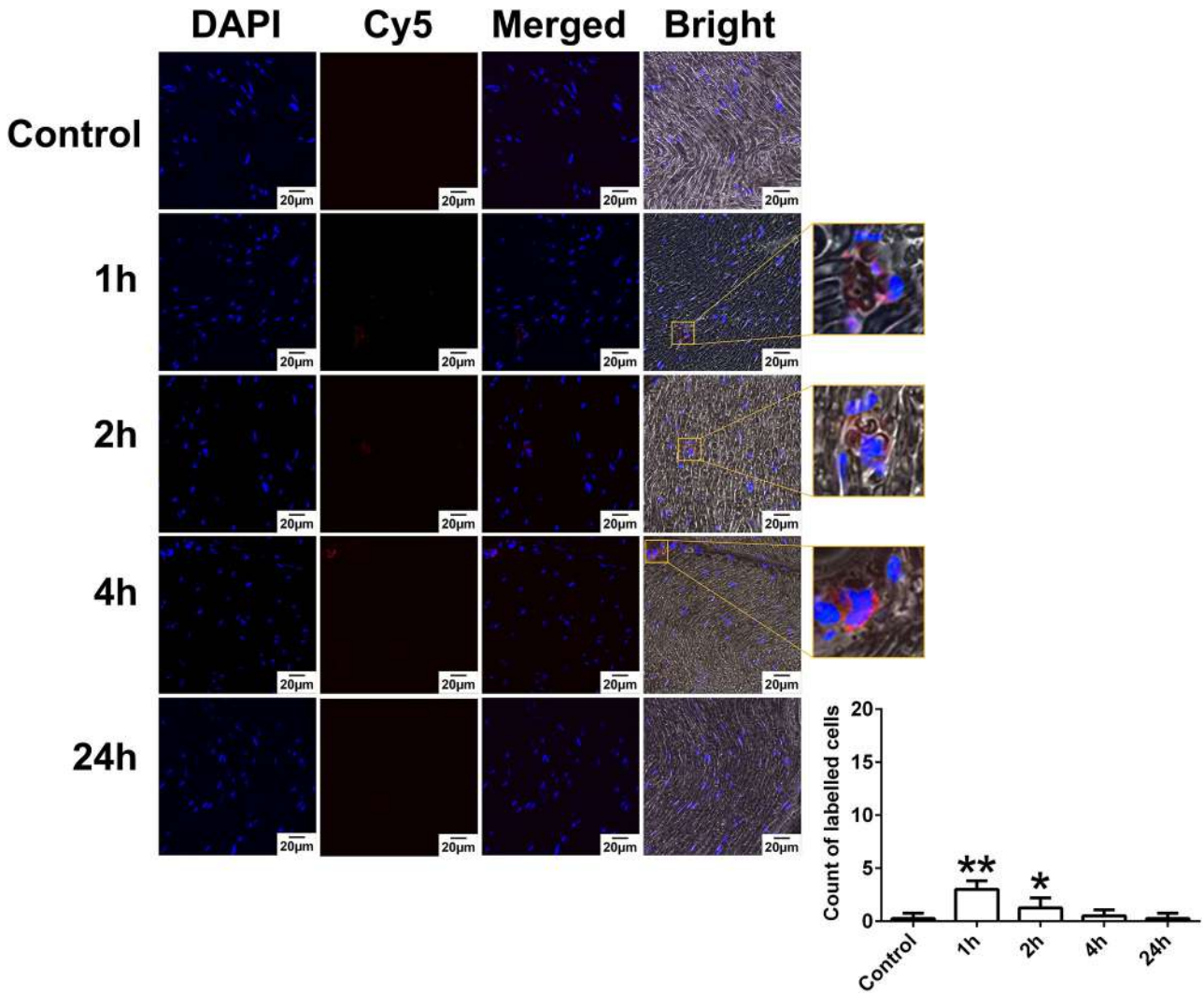

Figure 4. Immunohistochemistry of the co-localization of DAPI and Cy5 in the proximal nerve segments in the mice of crush nerve model. Following the topical treatment with Cy5-exosomes in the nerve crush site, the DAPI+/Cy5+ cells are quantified based on 20 randomly selected fields of the proximal nerve segments at 60× magnification, with results expressed as the average number of cells per field in the longitudinal section of the sciatic nerve. The symbols * and ** indicate significant changes ($P < 0.05$ and $P < 0.01$, respectively) compared to the control group. The error bars indicate the standard error from the mean. The length of the scale bar measures 10 μm.

spatial spots based on gene counts (Fig. 5B) and gene features (Fig. 5C) were plotted, highlighting the spatial distribution of specific gene counts and features in the spinal cords of ADSC-exo-treated and control mice. We employed the RCTD method to integrate the results of the spatial transcriptome and scRNA-seq analyses, which allowed us to identify the predominant cell types within each spatial spot (Fig. 5D). With each cell type in the spots represented by a different color, the ADSC-exo-treated group exhibited a noticeable shift in the cell type composition.

Figure 6 illustrates the distribution of various cell types in the spinal cord sections from the control (Fig. 6A) and ADSC-exo (Fig. 6B) groups. Each heatmap represents a different cell type, showing its relative abundance and localization within the tissue. Overall, the spatial distribution and density of various cell types within the spinal cord were similar, with only subtle differences between the two groups. The dot plot (Fig. 7A) shows the contrasting expression of crucial genes in neurons, oligodendrocytes, and Schwann cells between the control and ADSC-exo-treated groups. The dot size corresponds to the percentage of cells expressing the gene, whereas the intensity of the color indicates the average expression level. Table 1 and the bar graph in Fig. 7B show the average log2 fold change in gene expression for neurons, oligodendrocytes, and Schwann cells between the control and ADSC-exo-treated groups. There was a noticeable upregulation of several genes (red dots) in the neurons and Schwann cells following ADSC-exo treatment, highlighting the potential activation of neurogenic pathways. In contrast, specific genes (green dots) were significantly downregulated in the oligodendrocytes. In neurons, genes such as Cd300c2, Fndc11, Tbx5, Tmem232, and Vmn1r86 were markedly upregulated, indicating changes in neuronal activity and response to treatment. Schwann cells showed significant upregulation of genes, such as Adam26a, Ccer1, Clec4e, Col6a5, Krt12, and Mmp8, reflecting improved structural support and repair mechanisms. In contrast, oligodendrocytes exhibited the downregulation of genes such as 2010106E10Rik, Apol7a,

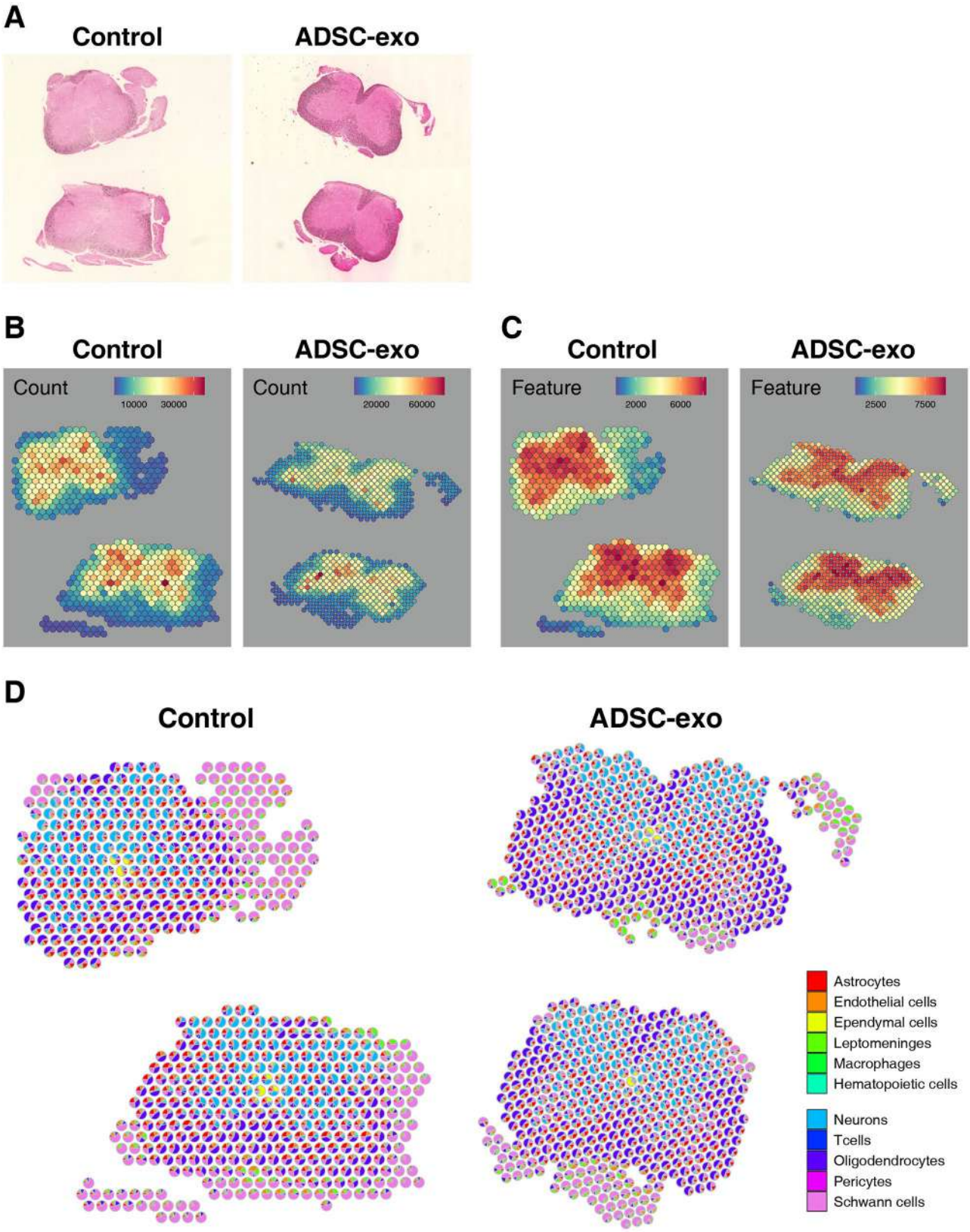

Figure 5. Spatial transcriptome analysis of spinal cord in control and ADSC-exo treated mice. (A) Histological sections of the spinal cord from both control and ADSC-exo treated mice, stained with H&E. (B) Heatmaps of spatial transcriptome count data. (C) Heatmaps of feature expression for both control and ADSC-exo treated groups. (D) The distribution of various predominant cell types within each spatial spot in the spinal cord sections of both control and ADSC-exo treated groups. Each color in the spots represents a different cell type.

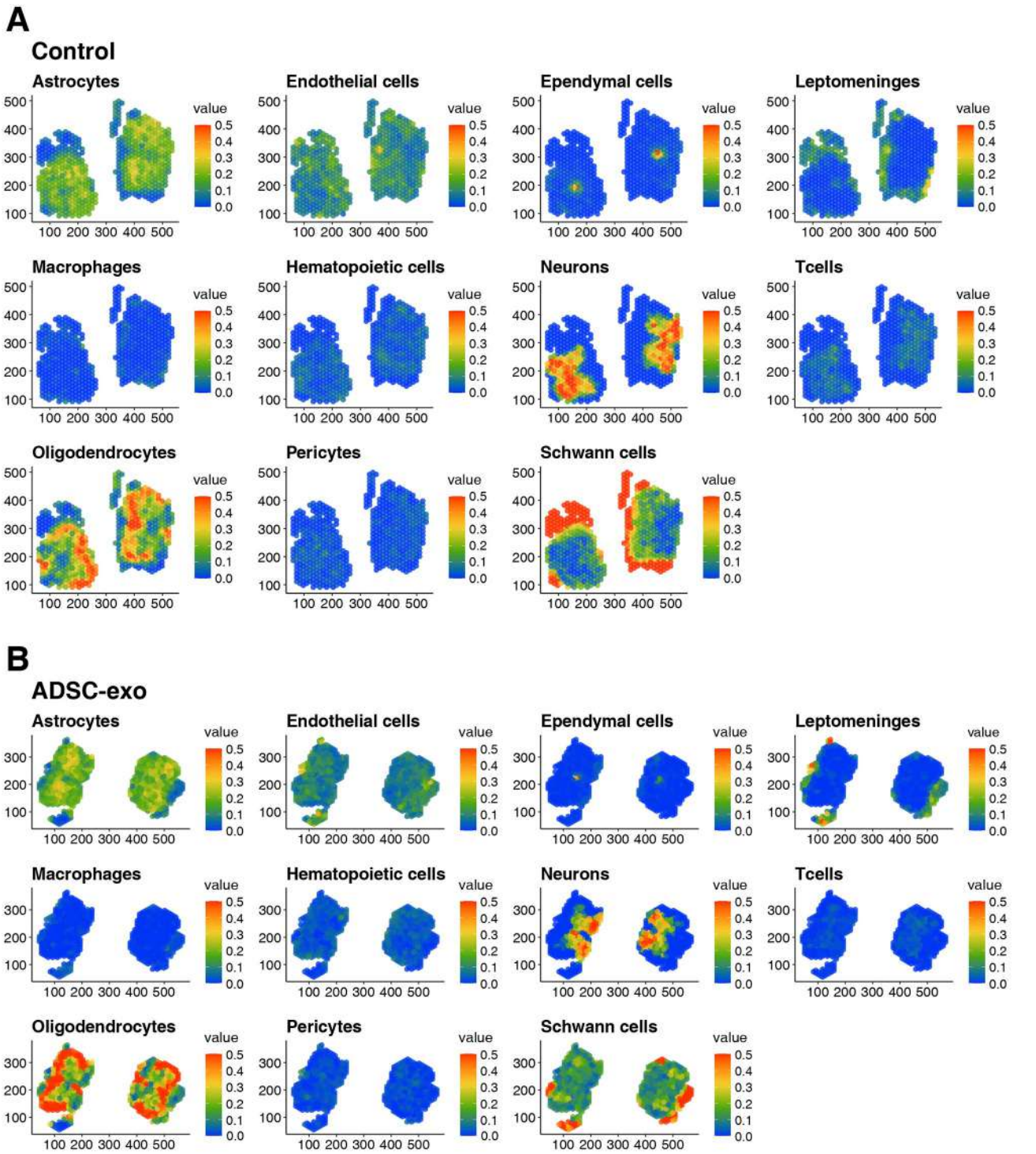

Figure 6. Cell type spatial distribution in control and ADSC-exo treated mice. Heatmaps showing the spatial distribution of various cell types in the control group (A) and the ADSC-exo-treated group (B).

Gja10, and Vmn1r87. A heatmap (Fig. 7C) and a river plot (Fig. 7D) of the expression of differentially expressed genes across neurons, oligodendrocytes, and Schwann cells in the control and ADSC exo-treated groups are shown.

Figure 8 shows the KEGG and GO enrichment analyses for neurons, oligodendrocytes, and Schwann cells. KEGG analysis revealed that the involved pathways were mainly in the Schwann cells, where enrichment in ECM-receptor interaction and focal adhesion pathways indicates improved cell adhesion and structural support. Enrichment of the PI3K-Akt signaling pathway suggests enhanced cell survival and growth, which are crucial for Schwann cell function and nerve repair. In oligodendrocytes,

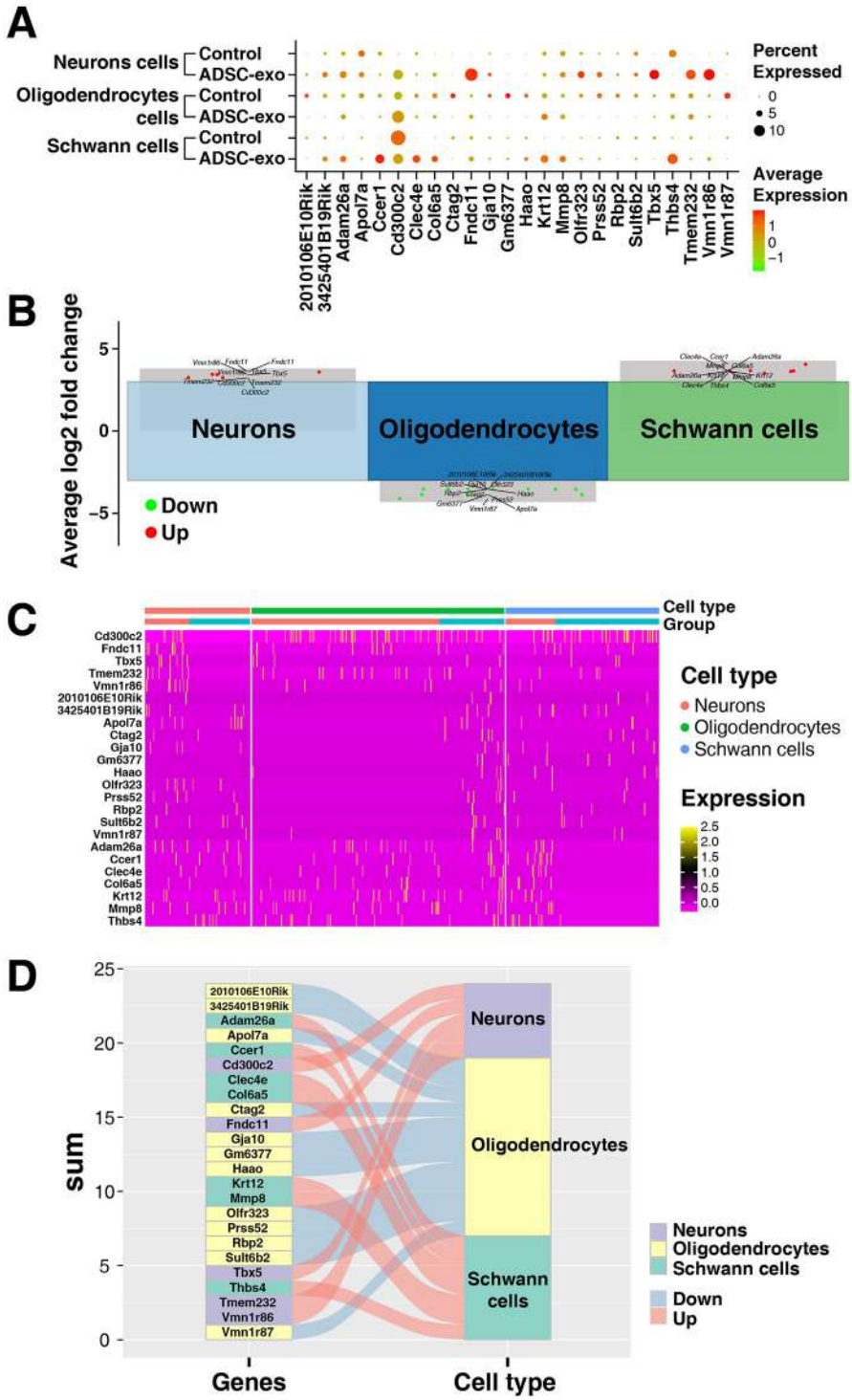

Figure 7. Differential expression genes in the spinal cord following ADSC-exo treatment. (A) Dot plot, (B) bar graph, (C) heatmap, and (D) river plot illustrate the differential expression of key genes between the control and ADSC-exo treated groups. Only the genes with an average log2 fold change in expression between ADSC-exo treated and control groups were displayed in the bar graph and river plot. The differentially expressed genes are only identified across three kinds of cells, including neurons, oligodendrocytes, and Schwann cells, between the control and ADSC-exo-treated groups.

enrichment in vitamin digestion and absorption suggests enhanced nutrient metabolism, which supports repair and regeneration. Increased tryptophan metabolism is indicative of improved neurotransmitter synthesis and health. Enhanced biosynthesis of cofactors highlights the increased production of essential molecules for enzymatic reactions. No KEGG-annotated pathways were found in neurons. Furthermore, GO enrichment analysis highlighted the biological processes (BP), cellular

Table 1

The significant differential expression genes in the spinal cord following ADSC-exo treatment versus that in the control group

Gene name	Access number	Log2 fold change	*P* value	Cell type
Cd300c2	NM_001303427.2	3.233	0.002	Neurons
Fndc11	NM_029281.4	3.595	0.000	Neurons
Tbx5	NM_080713.2	3.425	0.002	Neurons
Tmem232	NM_001083908.1	3.233	0.002	Neurons
Vmn1r86	NM_030783.1	3.425	0.001	Neurons
2010106E10Rik	NR_027053.1	–3.532	0.007	Oligodendrocytes
3425401B19Rik	NR_045722.1	–3.532	0.007	Oligodendrocytes
Apol7a	NM_009695.3	–3.854	0.002	Oligodendrocytes
Ctag2	NM_001164546.1	–3.854	0.002	Oligodendrocytes
Gja10	NM_001161719.2	–3.532	0.007	Oligodendrocytes
Gm6377	NR_027053.1	–3.854	0.002	Oligodendrocytes
Haao	NM_010421.2	–3.532	0.007	Oligodendrocytes
Olfr323	NM_001011782.1	–3.532	0.007	Oligodendrocytes
Prss52	NM_001168503.1	–3.854	0.002	Oligodendrocytes
Rbp2	NM_009030.4	–3.532	0.007	Oligodendrocytes
Sult6b2	NM_001081323.1	–3.532	0.007	Oligodendrocytes
Vmn1r87	NM_030784.1	–4.117	0.000	Oligodendrocytes
Adam26a	NM_033615.2	3.649	0.004	Schwann cells
Ccer1	NM_027693.2	4.064	0.000	Schwann cells
Clec4e	NM_021313.2	3.649	0.001	Schwann cells
Col6a5	NM_001145101.1	3.649	0.004	Schwann cells
Krt12	NM_010424.3	3.649	0.001	Schwann cells
Mmp8	NM_008608.1	3.649	0.004	Schwann cells
Thbs4	NM_011582.3	3.524	0.004	Schwann cells

components (CC), and molecular functions (MF) impacted by ADSC-exo treatment. In summary, the administration of ADSC-exos resulted in a notable enhancement of several biological processes, cellular components, and molecular functions in neurons, oligodendrocytes, and Schwann cells. These changes suggest that ADSC-exos promote enhanced metabolic activity, cell communication, and structural support, contributing to the overall regenerative environment of the spinal cord.

Regarding cell-cell interactions, the number and strength of interactions between different cell types in the control (Fig. 9A) and ADSC-Exo-treated groups are shown (Fig. 9B). The network diagram and heatmap show the interactions between various cell types, such as astrocytes, neurons, oligodendrocytes, Schwann cells, endothelial cells, leptomeninges, and ependymal cells. Supplemental Figure 1 (available at: http://links.lww.com/JS9/D614) shows heat maps representing the communication probability between different cell types in the spinal cord of the control and ADSC-exo-treated groups as well as an extended view of the ADSC-exo-treated groups. Communication probabilities were visualized based on the significance of the interactions and the intensity of the communication probability. ADSC-exo treatment significantly enhanced the probability of communication and the strength of interaction between various cell types in the spinal cord. The bar graph in Fig. 9 depicts the most significant interaction pairs contributing to the overall network. Interactions such as Ptpn-Gcg7m1 and Fgf1-Fgf2 played critical roles in both groups; however, the sequence of involvement of several pathways differed between the control and ADSC-exo therapy groups. Supplemental Figure 2 (available at: http://links.lww.com/JS9/D615) shows network and chord diagrams for seven of the most important signaling pathways, including prosaposin (PSAP), pleiotrophin (PTN), fibroblast growth factor (FGF), secreted phosphoprotein 1 (SPP1), SLIT And NTRK Like Family Member (SLITRK), vascular endothelial growth factor (VEGF), and growth arrest-specific protein (GAS), comparing the control and ADSC-exo treated groups. Each signaling pathway is illustrated through interactions between different cell types: astrocytes, neurons, oligodendrocytes, Schwann cells, endothelial cells, ependymal cells, and leptomeninges. Spatial transcriptome analysis of astrocytes revealed a marked increase in the connectivity and communication between astrocytes and other cell types in the spinal cord. The network diagrams in Fig. 9 further illustrate the enhanced role of astrocytes, showing increased connections and strengths of interaction with neurons, oligodendrocytes, and Schwann cells. The heat map in Supplemental Figure 1 (available at: http://links.lww.com/JS9/D614) indicates a higher number and strength of interactions involving astrocytes in the ADSC-exo-treated group than in the control group. This was particularly evident in the enhanced complexity and intensity of the signaling pathway networks shown in Supplemental Figure 2 (available at: http://links.lww.com/JS9/D615), where astrocytes (represented in red) demonstrated more robust participation in several key pathways after ADSC-exo treatment, notably in FGF, SPP1, VEGF, and SLITRK signaling. The overall increase in cell-cell interactions suggests the upregulation of genes involved in intercellular communication, growth factor production, and extracellular matrix remodeling. This heightened astrocytic activity likely contributes to creating a more supportive environment for nerve regeneration through multiple mechanisms, including increased production of neurotrophic factors, improved metabolic support for neurons and oligodendrocytes, enhanced structural remodeling of the extracellular matrix, and potential modulation of the inflammatory response. Overall, ADSC-exo treatment significantly enhanced the number and strength of the interactions between various cell types in the spinal cord, especially between Schwann cells and astrocytes.

Discussion

Anterograde and retrograde axonal transport are essential processes within neurons that facilitate the movement of various cellular components and materials along axons[39,40]. These transport mechanisms are essential for maintaining neuronal function and ensuring that neurons adapt to various physiological demands. Anterograde axonal transport involves the transfer of cellular components and substances from the neuronal cell body to the terminal synaptic ends of axons. This transport process is crucial for supplying the axon and its terminals with proteins, lipids, organelles, and other materials required for neurotransmission and axonal maintenance[41-43]. However, retrograde axonal transport involves the movement of cellular components and materials from the terminal branches of the axon back toward the neuronal cell body. This process serves various critical functions, including recycling and repair, signaling to prompt neurons to adjust their protein production, and defense[44-46].

It had been reported that the injection of labeled ADSC-exo into both proximal and distal sites around nerve injuries in adult Wistar rats results in the uptake of exosomes, suggesting that

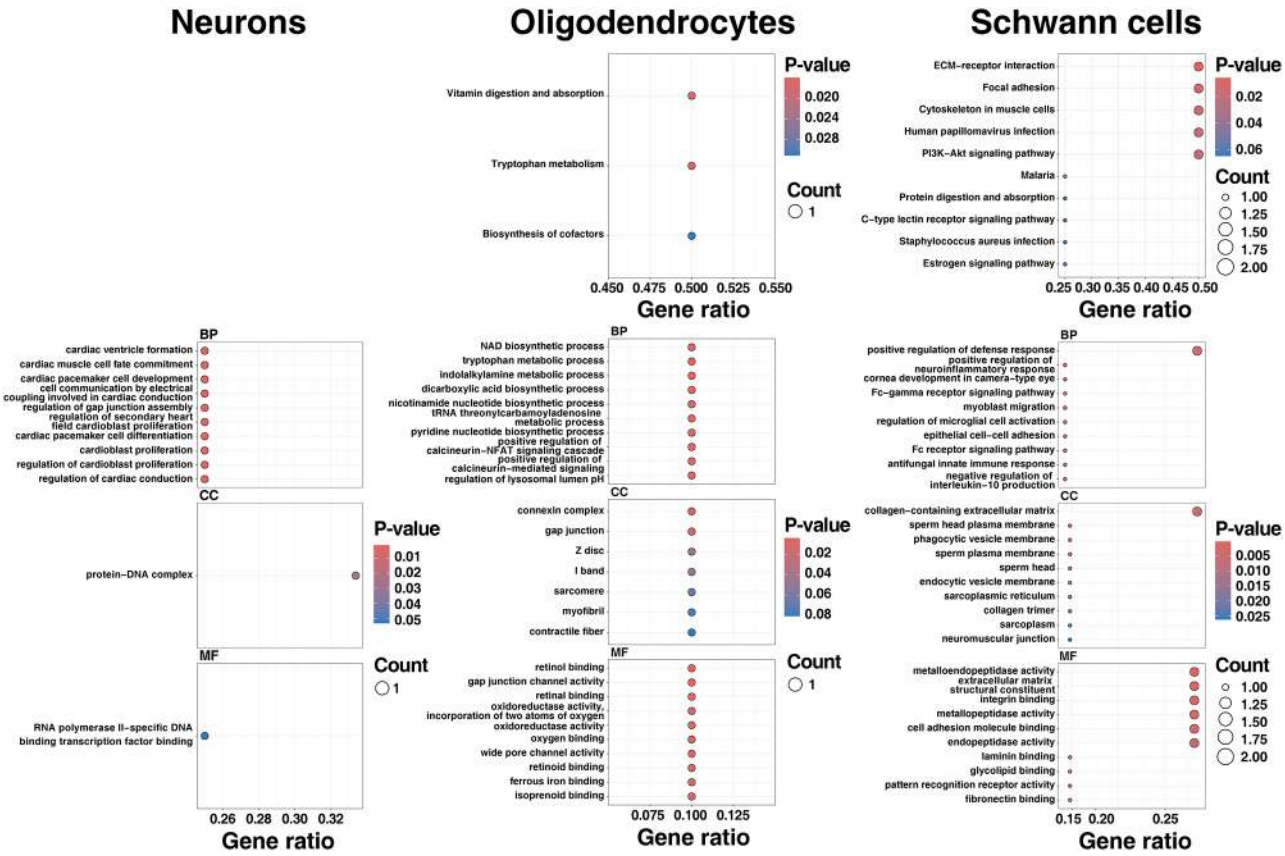

Figure 8. KEGG and Gene Ontology (GO) enrichment analysis. The upper raw lists the involvement of KEGG pathways, primarily in Schwann cells and oligodendrocytes, while the neurons show no KEGG-annotated pathways. The lower raw displays the biological processes (BP), cellular components (CC), and molecular functions (MF) in GO analysis for neurons, oligodendrocytes, and Schwann cells following ADSC-exo treatment.

ADSC-exo are internalized by regenerating fibers in vivo without being engulfed by macrophages[17]. Following peripheral nerve injury, ADSC-exos enhanced Schwann cell proliferation and reduced apoptosis by modulating Bcl-2 and Bax mRNA expression[16]. Researchers have investigated whether Schwann cells or dorsal root ganglion (DRG) neurons preferentially take up ADSC-exo in rats with sciatic nerve transection and with ADSC-exo filled in a silicone tube bridging the nerve gap. They found that Schwann cell uptake depended on the dose, whereas DRG neurons showed limited uptake[15]. However, ADSC-exos promoted axonal growth in DRG neurons[15].

In this study, we used confocal microscopy to observe and identify fluorescence-labeled exosomes in the innervated spinal cord and proximal nerve segments after spraying ADSC-exo onto the crushed sciatic nerve. Using spatial transcriptome analysis to investigate the microenvironment and molecular mechanisms, we observed a noticeable upregulation of genes in neurons and Schwann cells following ADSC-exo treatment. Notably, Schwann cells can dedifferentiate, proliferate, and migrate into the spinal cord after nerve injuries, particularly from the nerve roots, where they assist in regenerating and remyelinating damaged axons. Studies have shown that endogenous Schwann cells can invade spinal cord lesion sites and integrate with astrocytes to form repaired tissues, thus enhancing axonal regrowth and signal conduction[47]. In addition, transplanted Schwann cells in animal models have been found to support extensive axonal regeneration, remyelination, and functional recovery, particularly when combined with strategies to overcome the inhibitory environment of glial scar[48]. This migration and repair potential highlights the vital role of Schwann cells in both peripheral and central nervous system recovery following injury. In this study, KEGG analysis revealed that the pathways involved were mainly in Schwann Cells, and enrichment in ECM-receptor interactions and focal adhesion pathways indicated improved cell adhesion and structural support. GO enrichment analysis showed that ADSC-exos promoted higher metabolic activity, better cell communication, and structural support, all of which helped the spinal cord's overall regenerative environment. Spatially, cell communication showed that the cells in the spinal cord interacted primarily through PSAP, PTN, FGF, SPP1, SLITRK, VEGF, and GAS signaling pathways. A study of spatial transcriptomes showed that ADSC-exo treatment increased the number and strength of interactions between different cell types in the spinal cord, mainly between Schwann cells and astrocytes.

Overall, significant changes in the spatial distribution and density of various cell types within the spinal cord suggest that ADSC-exo treatment promotes a regenerative environment conducive to spinal cord repair and functional recovery. However, this study has some limitations that should be addressed. For

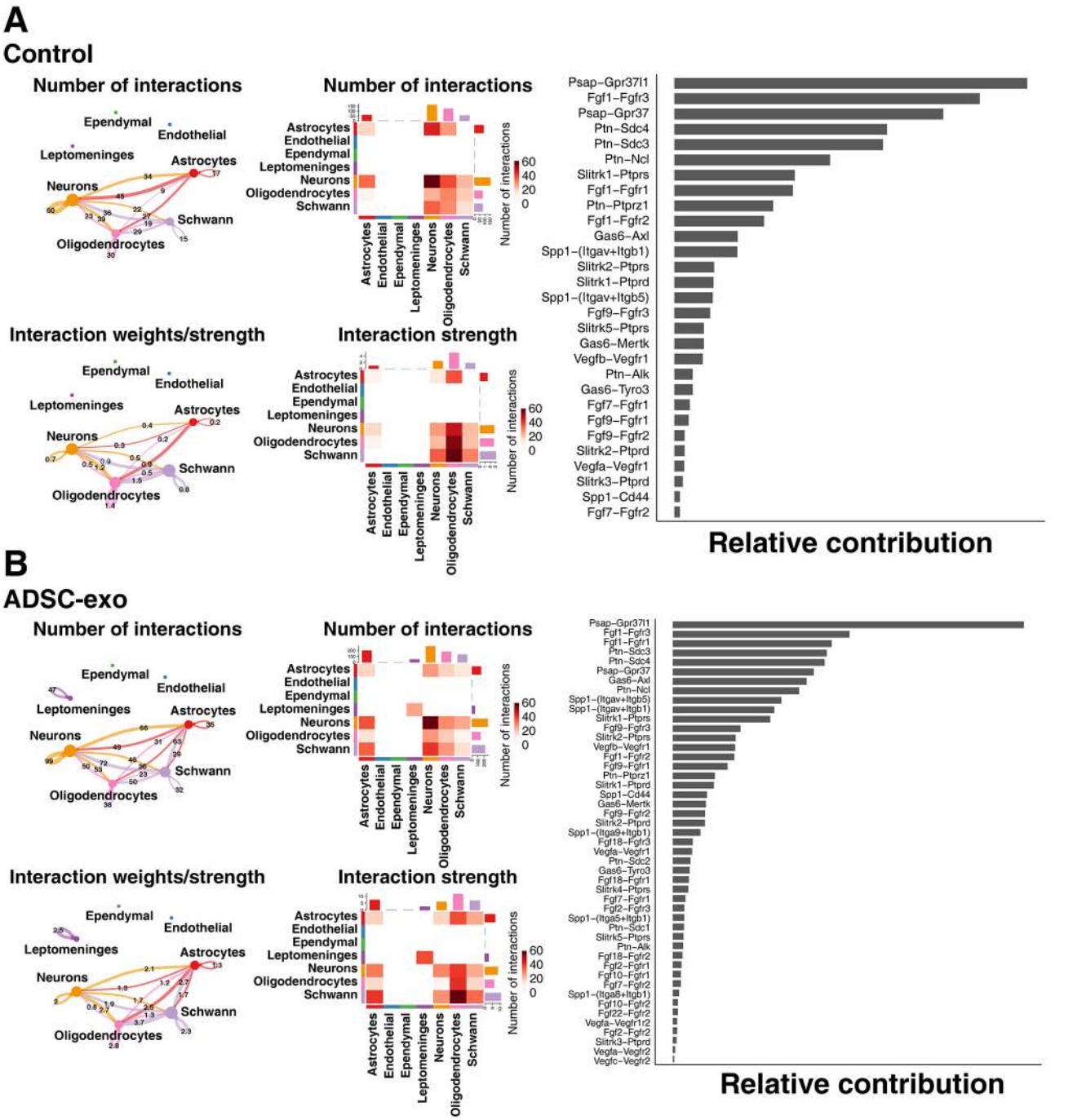

Figure 9. Cell-cell interaction. The cell-cell communication is visualized using CellChat and CellChatDB for a comprehensive database of ligand-receptor interactions and cell-cell communication networks. The network diagram shows the number and strength of interactions between different cell types, and the heatmap demonstrates the most significant interaction pairs that contribute to the overall network in the control group (A) and ADSC-exo-treated group (B).

example, in neurons, genes such as Cd300c2, Fndc11, Tbx5, Tmem232, and Vmn1r86 are markedly upregulated, while Schwann cells show significant upregulation of genes such as Adam26a, Ccer1, Clec4e, Col6a5, Krt12, and Mmp8. Although changes in these genes may reflect altered neuronal activity and responses to treatment, further research is required to investigate the actual mechanisms of these altered genes. Furthermore, the spatial transcriptome's capture area was 6.5 × 6.5 mm, with less than one thousand spots per capture area. Each spot had around one to five cells inside with a diameter of 55 μm. Therefore, the gene expression of the surrounding cells is more likely to influence cells with lower abundance and dispersed distribution, making them difficult to detect. Additionally, spatial transcriptome analysis designs the cell type for each spot based on the cell

type that registers the highest score, thereby excluding certain cell types such as NK cells or B cells from detection.

This study had some limitations. First, we focused on the L4-L6 spinal cord segments based on previous studies[23,49,50] demonstrating that these segments are the predominant source of sciatic nerve innervation. However, the exact location of the innervated neurons may vary between strains and may occur in L3; the involvement of L6 in mice is variable[51], resulting in differing interpretations of the findings. Furthermore, while numerous studies have shown that ADSC-exo can improve the regenerative capacity of neurons or Schwann cells and that the addition of ADSC-exo in vivo significantly increases nerve regeneration[15] and in our previous study[22], the impact of gene changes in these cells on regenerative capacity and especially the behavior recovery requires further investigation.

Conclusions

This study provides significant insights into the molecular mechanisms underlying the effects of ADSC-exos on nerve regeneration following crush injury. Through the innovative use of fluorescent labeling and spatial transcriptomics, we demonstrated the presence of ADSC-exo in spinal neurons and proximal nerve segments and revealed their wide-ranging impacts on gene expression and cell-cell interactions. The observed upregulation of key genes in neurons and Schwann cells, coupled with enhanced cell communication and metabolic activity, suggests that ADSC-exos promote a regenerative environment conducive to nerve repair. The involvement of multiple signaling pathways and cell types highlights the complex nature of the regenerative response. While these findings advance our understanding of ADSC exo-mediated nerve regeneration, further research is necessary to fully elucidate the underlying mechanisms and translate these insights into clinical applications.

Ethical approval

The Institutional Animal Care and Use Committee (IACUC) at Kaohsiung Chang Gung Memorial Hospital, Taiwan, has granted approval for the protocols that regulate the housing conditions, surgical procedures, pain relief, and evaluations (Reference number: 2022031502).

Consent

Not applicable.

Sources of funding

This research was supported by Chang Gung Memorial Hospital, grant number CMRPG8L0201, CMRPG8M0141, and CMRPG8M0921 to Cheng-Shyuan Rau.

Author's contribution

Writing – original draft preparation, C.-S.R.; Writing – review & editing, S.-C.W.; Validation, P.-J.K.; Visualization, C.-W.L.; Resources, T.-H.L.; Methodology, Y.-C.W; Software, C.-W.T.; Funding acquisition, C.-S.R.; Conceptualization, C.-H.H. All authors have read and agreed to the published version of the manuscript.

Conflicts of interest disclosure

All the authors declare to have no conflicts of interest relevant to this study.

Research registration unique identifying number (UIN)

Not applicable.

Guarantor

Ching-Hua Hsieh.

Provenance and peer review

Not applicable.

Data availability statement

Not applicable.

Acknowledgments

We appreciate the support provided by the Genomic & Proteomic Core Laboratory, Department of Medical Research, Kaohsiung Chang Gung Memorial Hospital.

References

[1] Lopes B, Sousa P, Alvites R, *et al*. Peripheral nerve injury treatments and advances: one health perspective. Int J Mol Sci 2022;23:918.
[2] Yegiyants S, Dayicioglu D, Kardashian G, Panthaki ZJ. Traumatic peripheral nerve injury: a wartime review. J Craniofac Surg 2010;21:998–1001.
[3] Garg K, Sinha S, Satyarthee GD, *et al*. Microsurgical outcome of post-traumatic peripheral nerve injuries: an experience of 23 cases and review of literature. Turk Neurosurg 2016;26:297–301.
[4] Murovic JA. Lower-extremity peripheral nerve injuries: a Louisiana State University Health Sciences Center literature review with comparison of the operative outcomes of 806 Louisiana State University Health Sciences Center sciatic, common peroneal, and tibial nerve lesions. Neurosurgery 2009;65:A18–23.
[5] Murovic JA. Upper-extremity peripheral nerve injuries: a Louisiana State University Health Sciences Center literature review with comparison of the operative outcomes of 1837 Louisiana State University Health Sciences Center median, radial, and ulnar nerve lesions. Neurosurgery 2009;65:A11–7.
[6] Robinson LR. Traumatic injury to peripheral nerves. Muscle Nerve 2022;66:661–70.
[7] Armas-Salazar A, García-Jerónimo AI, Villegas-López FA, Navarro-Olvera JL, Carrillo-Ruiz JD. Clinical outcomes report in different brachial plexus injury surgeries: a systematic review. Neurosurg Rev 2022;45:411–19.
[8] McGillivray MK, Haldane C, Doherty C, Berger MJ. Evaluation of muscle strength following peripheral nerve surgery: a scoping review. Pm R 2021;14:383–394.
[9] Modrak M, Talukder MAH, Gurgenashvili K, Noble M, Elfar JC. Peripheral nerve injury and myelination: potential therapeutic strategies. J Neurosci Res 2020;98:780–95.
[10] Wang ML, Rivlin M, Graham JG, Beredjiklian PK. Peripheral nerve injury, scarring, and recovery. Connective Tissue Res 2019;60:3–9.

[11] Jiang L, Zheng Y, Chen O, Chu T, Ding J, Yu Q. Nerve defect repair by differentiated adipose-derived stem cells and chondroitinase ABC-treated acellular nerves. Int J Neurosci 2016;126:568–76.
[12] Reid AJ, Sun M, Wiberg M, Downes S, Terenghi G, Kingham PJ. Nerve repair with adipose-derived stem cells protects dorsal root ganglia neurons from apoptosis. Neuroscience 2011;199:515–22.
[13] Fu XM, Wang Y, Fu WL, *et al*. The combination of adipose-derived Schwann-like cells and acellular nerve allografts promotes sciatic nerve regeneration and repair through the JAK2/STAT3 signaling pathway in rats. Neuroscience 2019;422:134–45.
[14] György B, Szabó TG, Pásztói M, *et al*. Membrane vesicles, current state-of-the-art: emerging role of extracellular vesicles. Cell Mol Life Sci 2011;68:2667–88.
[15] Chen J, Ren S, Duscher D, *et al*. Exosomes from human adipose-derived stem cells promote sciatic nerve regeneration via optimizing Schwann cell function. J Cell Physiol 2019;234:23097–110.
[16] Liu CY, Yin G, Sun YD, *et al*. Effect of exosomes from adipose-derived stem cells on the apoptosis of Schwann cells in peripheral nerve injury. CNS Neurosci Ther 2020;26:189–96.
[17] Bucan V, Vaslaitis D, Peck CT, Strauß S, Vogt PM, Radtke C. Effect of exosomes from rat adipose-derived mesenchymal stem cells on neurite outgrowth and sciatic nerve regeneration after crush injury. Mol Neurobiol 2019;56:1812–24.
[18] Yang J, Wang B, Wang Y, *et al*. Exosomes derived from adipose mesenchymal stem cells carrying miRNA-22-3p promote Schwann cells proliferation and migration through downregulation of PTEN. Dis Markers 2022;2022:7071877.
[19] Huang X, Ding J, Li Y, *et al*. Exosomes derived from PEDF modified adipose-derived mesenchymal stem cells ameliorate cerebral ischemia-reperfusion injury by regulation of autophagy and apoptosis. Exp Cell Res 2018;371:269–77.
[20] Yin G, Yu B, Liu C, *et al*. Exosomes produced by adipose-derived stem cells inhibit Schwann cells autophagy and promote the regeneration of the myelin sheath. Int J Biochem Cell Biol 2021;132:105921.
[21] Farinazzo A, Turano E, Marconi S, Bistaffa E, Bazzoli E, Bonetti B. Murine adipose-derived mesenchymal stromal cell vesicles: in vitro clues for neuroprotective and neuroregenerative approaches. Cytotherapy 2015;17:571–78.
[22] Rau P-JK C-S, Kuo P-J, Wu S-C, *et al*. Enhanced nerve regeneration by exosomes secreted by adipose-derived stem cells with or without FK506 stimulation. Int J Mol Sci 2021;22:8545.
[23] Kuo P-J, Rau C-S, Wu S-C, *et al*. Exosomes secreted by adipose-derived stem cells following FK506 stimulation reduce autophagy of macrophages in spine after nerve crush injury. Int J Mol Sci 2021;22:9628.
[24] Kilkenny C, Browne WJ, Cuthill IC, Emerson M, Altman DG. Improving bioscience research reporting: the ARRIVE guidelines for reporting animal research. PLoS Biol 2010;8:e1000412.
[25] Lee TS, Kim Y, Zhang W, Song IH, Tung CH. Facile metabolic glycan labeling strategy for exosome tracking. Biochim Biophys Acta Gen Subj 2018;1862:1091–100.
[26] Song S, Shim MK, Lim S, *et al*. In situ one-step fluorescence labeling strategy of exosomes via bioorthogonal click chemistry for real-time exosome tracking in vitro and in vivo. Bioconjug Chem 2020;31:1562–74.
[27] Théry C, Witwer KW, Aikawa E, *et al*. Minimal information for studies of extracellular vesicles 2018 (MISEV2018): a position statement of the International Society for Extracellular Vesicles and update of the MISEV2014 guidelines. J Extracell Vesicles 2018;7:1535750.
[28] Witwer KW, Goberdhan DC, O'Driscoll L, *et al*. Updating MISEV: evolving the minimal requirements for studies of extracellular vesicles. J Extracell Vesicles 2021;10:e12182.
[29] Wu SC, Kuo PJ, Rau CS, *et al*. Increased angiogenesis by exosomes secreted by adipose-derived stem cells upon lipopolysaccharide stimulation. Int J Mol Sci 2021;22:8877.
[30] Huang L-H, Rau C-S, Wu S-C, *et al*. Identification and characterization of hADSC-derived exosome proteins from different isolation methods. J Cell Mol Med 2021;25:7436–50.
[31] Hsieh CH, Rau CS, Kuo PJ, *et al*. Knockout of toll-like receptor impairs nerve regeneration after a crush injury. Oncotarget 2017;8:80741–56.
[32] Wu SC, Rau CS, Lu TH, *et al*. Knockout of TLR4 and TLR2 impair the nerve regeneration by delayed demyelination but not remyelination. J Biomed Sci 2013;20:62.
[33] Yan Y, Sun HH, Mackinnon SE, Johnson PJ. Evaluation of peripheral nerve regeneration via in vivo serial transcutaneous imaging using transgenic Thy1-YFP mice. Exp Neurol 2011;232:7–14.
[34] Magill CK, Moore AM, Yan Y, *et al*. The differential effects of pathway-versus target-derived glial cell line-derived neurotrophic factor on peripheral nerve regeneration. J Neurosurg 2010;113:102–09.
[35] Myckatyn TM, Mackinnon SE, Hunter DA, Brakefield D, Parsadanian A. A novel model for the study of peripheral-nerve regeneration following common nerve injury paradigms. J Reconstr Microsurg 2004;20:533–44.
[36] Magill CK, Tong A, Kawamura D, *et al*. Reinnervation of the tibialis anterior following sciatic nerve crush injury: a confocal microscopic study in transgenic mice. Exp Neurol 2007;207:64–74.
[37] Chen J, Liu W, Luo T, *et al*. A comprehensive comparison on cell-type composition inference for spatial transcriptomics data. Brief Bioinform 2022;23:bbac245.
[38] Matson KJE, Russ DE, Kathe C, *et al*. Single cell atlas of spinal cord injury in mice reveals a pro-regenerative signature in spinocerebellar neurons. Nat Commun 2022;13:5628.
[39] Hirokawa N, Takemura R. Molecular motors in neuronal development, intracellular transport and diseases. Curr Opin Neurobiol 2004;14:564–73.
[40] Saxton WM, Hollenbeck PJ. The axonal transport of mitochondria. J Cell Sci 2012;125:2095–104.
[41] Hirokawa N, Niwa S, Tanaka Y. Molecular motors in neurons: transport mechanisms and roles in brain function, development, and disease. Neuron 2010;68:610–38.
[42] De Vos KJ, Hafezparast M. Neurobiology of axonal transport defects in motor neuron diseases: opportunities for translational research? Neurobiol Dis 2017;105:283–99.
[43] Kapitein LC, Hoogenraad CC. Building the neuronal microtubule cytoskeleton. Neuron 2015;87:492–506.
[44] Millecamps S, Julien JP. Axonal transport deficits and neurodegenerative diseases. Nat Rev Neurosci 2013;14:161–76.
[45] White JA, Banerjee R, Gunawardena S. Axonal transport and neurodegeneration: how marine drugs can be used for the development of therapeutics. Mar Drugs 2016;14:102.
[46] Perlson E, Maday S, Fu -M-M, Moughamian AJ, Holzbaur ELF. Retrograde axonal transport: pathways to cell death? Trends Neurosci 2010;33:335–44.
[47] Zhang SX, Huang F, Gates M, Holmberg EG. Role of endogenous Schwann cells in tissue repair after spinal cord injury. Neural Regen Res 2013;8:177–85.
[48] Oudega M, Xu XM. Schwann cell transplantation for repair of the adult spinal cord. J Neurotrauma 2006;23:453–67.
[49] Fan M, Mi R, Yew DT, Chan WY. Analysis of gene expression following sciatic nerve crush and spinal cord hemisection in the mouse by microarray expression profiling. Cell Mol Neurobiol 2001;21:497–508.
[50] Velandia ML, Montoya JV, Martínez M, Perdomo S, Castellanos JE. Comparison of three neuro-tracing techniques for identification of the sciatic spinal nerve origin in mice. Biomedica 2002;22:529–34.
[51] Rigaud M, Gemes G, Barabas ME, *et al*. Species and strain differences in rodent sciatic nerve anatomy: implications for studies of neuropathic pain. Pain 2008;136:188–201.